Supporting Information for "SERMeQ model produces realistic retreat of 155 Greenland outlet glaciers"

Lizz Ultee[1] and Jeremy Bassis[2]

[1]Department of Earth, Atmospheric, and Planetary Sciences, Massachusetts Institute of Technology, Cambridge, MA, USA.

[2]Department of Climate & Space Sciences, University of Michigan, Ann Arbor, MI, USA.

Contents

Additional Supporting Information (Files uploaded separately)

1. Table S1, a list of all Greenland outlet glaciers in the MEaSUREs dataset with their glacier ID number, name(s), optimal yield strength found, and notes on inclusion in the analysis. The note "Flagged for bad flowline trace" indicates glaciers that required manual intervention to complete data processing, but which are now included in the analysis.

Introduction

Text S1. Ice dynamics in SERMeQ

The ice dynamics in our model are based on a perfectly-plastic limiting case of a viscoplastic rheology (Bassis & Ultee, 2019). This rheology describes a glacier with two characteristic timescales: viscous deformation (slow) and mass loss by calving (fast). Modifications to the simple plastic formulation allow calving at a grounded ice-water interface (Ultee & Bassis, 2016) and interaction between multiple tributary glaciers (Ultee & Bassis, 2017). By requiring instantaneous stress balance across the glacier terminus, this formulation finds that the ice thickness H_{terminus} at a given terminus position, in water of depth D, is limited by the yield strength and cannot exceed the yield thickness,

$$H_{\text{y}} = 2\frac{\tau_{\text{y}}}{\rho_{\text{i}}g} + \sqrt{\frac{\rho_{\text{w}}}{\rho_{\text{i}}}D^2 + 2\frac{\tau_{\text{y}}}{\rho_{\text{i}}g}}, \qquad (S1)$$

with τ_{y} the yield strength of glacier ice, $\rho_{\text{i}} = 920$ kg m^{-3} the density of glacier ice, $\rho_{\text{w}} = 1020$ kg m^{-3} the density of seawater, and $g = 9.81$ m s^{-2} the acceleration due to gravity (Ultee & Bassis, 2016).

In a perfectly plastic glacier (Nye, 1951), the upstream ice thickness H along a central flowline, with along-flow direction x and ice surface elevation s, is also controlled by the yield strength:

$$H\frac{\partial s}{\partial x} = \frac{\tau_{\text{y}}}{\rho_{\text{i}}g}. \qquad (S2)$$

This approximation corresponds to a case where the glacier bed is (nearly) plastic and the glacier stress balance is dominated by shear at the glacier bed and valley walls—appropriate for most Greenland outlet glaciers. We also account for longitudinal

stresses in a boundary layer near the terminus, where they are more likely to be important (Bassis & Ultee, 2019).

Finally, we use mass continuity to derive an expression for the rate of terminus advance or retreat due to calving (see Text S2, below). With each change in terminus position, we calculate a new surface profile according to Equations S1-S2, and we integrate the changes in ice volume above buoyancy throughout the catchment to deduce a contribution to global mean sea level. Figure S1 shows an example sequence of glacier profiles and corresponding sea level contribution as calculated by SERMeQ.
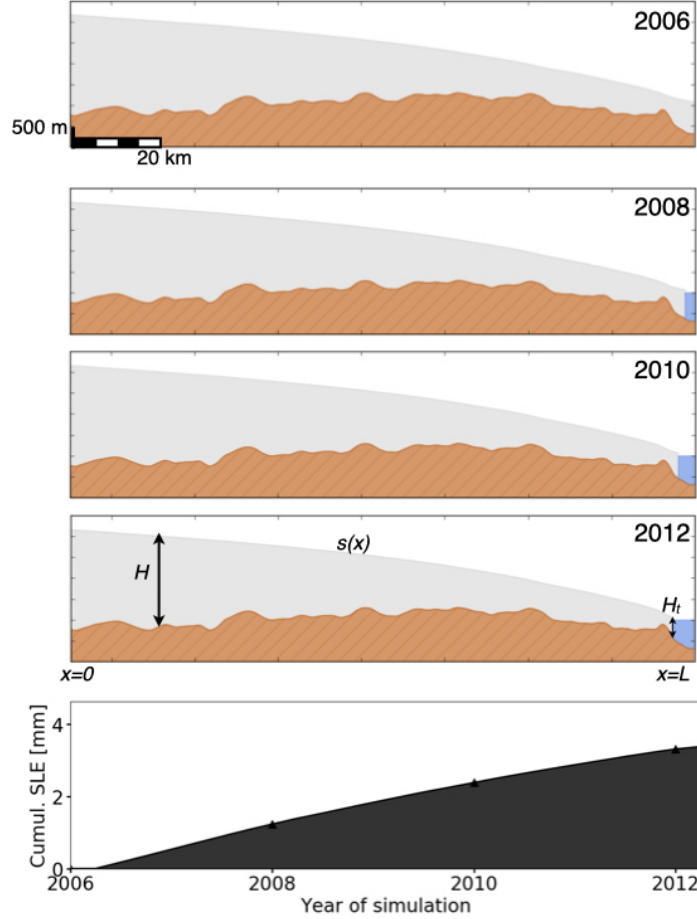

Figure S1. Surface profiles produced by SERMeQ along a flowline in the central part of Sermeq Kujalleq's catchment, with corresponding cumulative sea level contribution (SLE) below. Profiles show glacier ice in grey, bedrock in brown, and fjord water in blue. Spatial scale is indicated on the 2006 panel and consistent throughout. Labels on 2012 panel indicate along-flow direction x, ice surface elevation $s(x)$, ice thickness H, terminus ice thickness H_t, and terminus location $x{=}L$ as used in Equations S1-S6. Cumulative SLE on bottom panel reflects catchment-integrated loss of ice volume above buoyancy converted to an equivalent volume of seawater and distributed over the area of the global ocean.

Despite the simplicity of the model, preliminary experiments have shown promise in reproducing both surface elevation profiles and advance/retreat rates of glaciers in Alaska and Greenland (Ultee & Bassis, 2016, 2017). However, our model only applies to grounded glaciers and cannot simulate the dynamics of floating ice tongues or shelves.

Text S2. Time evolution of the terminus position

Glacier terminus position in SERMeQ evolves in response to near-terminus stretching, bedrock topography, and changes in catchment-wide surface mass balance as described in Ultee (2018) and Bassis and Ultee (2019). Below is a brief summary derivation of the terminus evolution condition as implemented in SERMeQ code.

Let $x = 0$ represent the ice divide and $x = L$ the terminus, where $L = L(t)$ is the length of the glacier (labelled in Figure S1). The time derivative dL/dt then represents the change in terminus position over time.

Taking the material derivative of the terminus ice thickness $H = H_y$ (constrained by Equation S1), we find

$$\frac{DH}{Dt}\bigg|_{x=L} = \frac{DH_y}{Dt}$$
$$\left[\frac{\partial H}{\partial t} + \frac{dL}{dt}\frac{\partial H}{\partial x}\right]_{x=L} = \frac{\partial H_y}{\partial t} + \frac{dL}{dt}\frac{\partial H_y}{\partial x}$$
$$\frac{\partial H}{\partial t}\bigg|_{x=L} = \frac{dL}{dt}\left[\frac{\partial H_y}{\partial x} - \frac{\partial H}{\partial x}\right]_{x=L} . \tag{S3}$$

Mass continuity requires

$$\frac{\partial H}{\partial t} + \frac{\partial}{\partial x}(HU) = \dot{a} \tag{S4}$$

where $H = H(x,t)$ is the ice thickness, $U = U(x,t)$ the ice velocity, and $\dot{a} = \dot{a}(x,t)$ the net ice accumulation rate, for all (x,t).

Substituting equation (S4) into (S3), we find

$$\dot{a} - H\frac{\partial U}{\partial x} - U\frac{\partial H}{\partial x} = \frac{dL}{dt}\left[\frac{\partial H_y}{\partial x} - \frac{\partial H}{\partial x}\right]_{x=L} \tag{S5}$$
$$\frac{dL}{dt} = \frac{\dot{a} - H\frac{\partial U}{\partial x} - U\frac{\partial H}{\partial x}}{\frac{\partial H_y}{\partial x} - \frac{\partial H}{\partial x}} , \tag{S6}$$

with all terms of equation (S6) evaluated at $x = L$, the terminus of the glacier (compare with Equation 54 of Bassis and Ultee (2019)). With the exception of ice accumulation rate $\dot{a}$, all terms are determined by the rheology of ice.

Upstream from the terminus, we assume a plastic yielding layer at the bed of the glacier. A perfectly plastic glacier would have a rigid ice plug above the yielding layer, but the perfect plastic approximation is a limiting case of several other rheologies that could be used to describe the slow deformation of ice in a pseudo-plug (e.g. Balmforth et al., 2006). Here we choose to describe the slow deformation of intact ice with the familiar Glen's flow law. At the terminus, as in Ultee and Bassis (2016, 2017), we require a vertical yield surface to describe the more rapid motion of fractured, disarticulated ice as it calves away from the intact glacier. This implies that the effective stress in a region of length δ upstream from the terminus is within ϵ of the yield strength τ_y. Near the terminus, we have

$$\frac{\partial U}{\partial x} = \dot{\varepsilon}_{xx} = A\tau_{xx}^n$$
$$= A\tau_y^n , \tag{S7}$$

where flow law exponent $n = 3$ and A is the flow rate parameter of Glen's flow law.

We integrate equation (S4) in x to find

$$\int_0^L \frac{\partial H}{\partial t}\,\mathrm{d}x + (HU)|_{x=L} = \int_0^L \dot{a}\,\mathrm{d}x \tag{S8}$$

$$U(x=L) = \frac{1}{H_{\text{terminus}}}\int_0^L \left[\dot{a} - \frac{\partial H}{\partial t}\right]\,\mathrm{d}x, \tag{S9}$$

and by the chain rule $\frac{\partial H}{\partial t} = \frac{\partial H}{\partial L}\frac{dL}{dt}$. Separating the integral in equation (S9) and expanding $\frac{\partial H}{\partial t}$ gives

$$U(x=L) = \frac{\dot{\alpha}L}{H_{\text{terminus}}} - \frac{dL}{dt}\frac{1}{H_{\text{terminus}}}\int_0^L \frac{\partial H}{\partial L}\,\mathrm{d}x, \tag{S10}$$

where $\dot{\alpha} = \frac{1}{L}\int_0^L \dot{a}\,\mathrm{d}x$ is the spatially-averaged ice accumulation rate along the flowline.

We now substitute our expressions (S7, S10) in to equation (S4) and rearrange to find

$$\frac{dL}{dt} = \frac{\dot{a} - A\tau_{\text{y}}^3 H_{\text{terminus}} + \frac{\dot{\alpha}L}{H_{\text{terminus}}}\frac{\partial H}{\partial x}}{\frac{\partial H_{\text{y}}}{\partial x} - \frac{\partial H}{\partial x}\left(1 - \frac{1}{H_{\text{terminus}}}\int_0^L \frac{\partial H}{\partial L}\right)}. \tag{S11}$$

We implement a discretized version of Equation S11 to describe the time evolution of glacier terminus position in SERMeQ.

Text S3. The role of adjustable parameters

Yield strength τ_{y}

For each glacier, we optimize the yield strength τ_y to find the best fit between a reconstructed and observed centerline surface elevation profile. Glaciers with flatter surface slopes, including those close to flotation, are best fit by lower values of τ_{y}. Steeper surface slopes are better fit by higher values of the yield strength. The optimization procedure is discussed in more detail in Ultee and Bassis (2016). The optimal value of τ_{y} found for each glacier is listed in Supplementary Table 1. There is no correlation between optimal yield strength and glacier latitude, and no other spatial pattern is evident.

Figure S2 shows a histogram of the best-fit values of τ_{y} obtained for the Greenland outlets we simulated. A central peak in the distribution shows that approximately 1/3 of the glaciers we simulate have an optimal yield strength between 125 kPa and 150 kPa. A smaller peak shows that there are also several glaciers in our set best fit by yield strengths between 5 kPa-25 kPa.

In this work, we have used a single value of τ_{y} at both the ice-bed interface and the calving front. It is plausible that the ice-bed interface could be deforming more readily than the pure ice at the calving front, for example if the glacier bed is composed of saturated marine sediments or if the ice is very close to flotation. Such a case would lead to low ice surface slopes and a low optimal value of τ_{y}, even though pure ice throughout the glacier may be stronger. We discuss the case of $\tau_{\text{bed}} < \tau_{\text{ice}}$ in Bassis and Ultee (2019).

Ice temperature T

The ice temperature T is used to select an appropriate value of the flow-rate parameter A in Glen's flow law. Here, we use an ice temperature constant in space and time and do not optimize for its value. In our previous work, we have found that warmer ice ($T = -2°$ C) is softer and more prone to rapid retreat. Conversely, colder ice ($T = -30°$ C) is stiffer and retreats more slowly. For more details, we refer the interested reader to Ultee (2018).
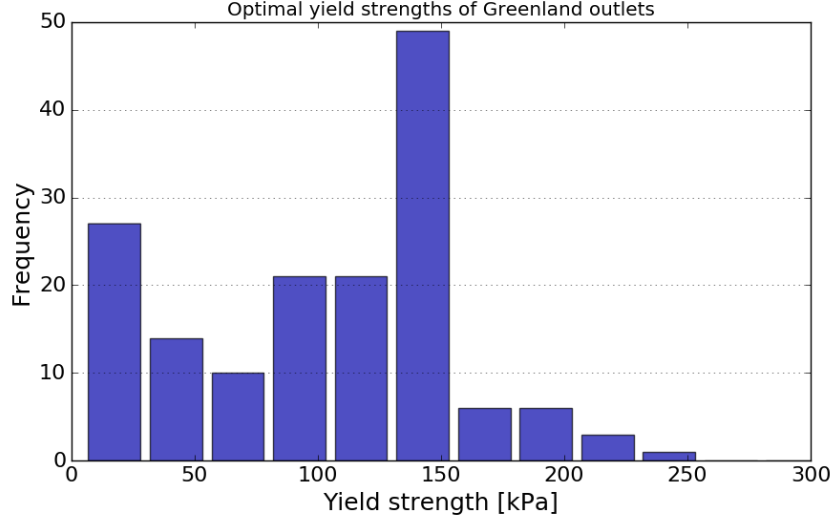
Figure S2. Histogram of optimal yield strength value found for each glacier.

Text S4. Inclusion of submarine melt

We do not explicitly simulate loss of ice from glacier termini by submarine melting. Rather, we have constructed an upper-bound estimate of retreat that is consistent with high submarine melt rates. Our requirement that effective stress near the glacier terminus must equal the yield strength of ice (see Text S1) makes an implicit constraint on the submarine melt rate, because the rate of submarine melt shapes the stress field near glacier termini (Ma, 2018; Ma & Bassis, 2019). There are three cases to consider:

Case I The submarine melt rate is very small compared with the terminus velocity, $u_s \ll u_t$. In this case, the terminus would be able to advance and thin episodically. However, advance and thinning would lower the effective stress at the glacier terminus, such that it would fall below the yield strength of ice and no longer satisfy our criterion. We therefore disallow Case I.

Case II The submarine melt rate is comparable to the terminus velocity, $u_s \sim u_t$. In this case submarine melt would balance the tendency of ice near the terminus to stretch and thin, maintaining the terminus ice thickness at the yield thickness.

Case III The submarine melt rate is very large compared with the terminus velocity, $u_s \gg u_t$. In this case, the erosion of the terminus by high submarine melt would create an overhang and promote calving (Ma & Bassis, 2019). Considered at long enough time scales, e.g. the 0.25 annum standard time step in SERMeQ rather than the hours to days considered in finer-scale process models, high submarine melting and enhanced calving would also maintain the terminus ice thickness at the yield thickness.

Both Cases II and III are consistent with our assumption that there is a yielding boundary layer at the glacier front that constrains the terminus ice thickness (see Bassis & Ultee, 2019). The maximum rate of length change computed in Equation 1 is compatible with both cases, and the ice mass lost in each time step can be considered a combination of mass lost to calving and to submarine melting.

The upper-bound retreat rate that we have sought in this work does not require explicit simulation of the submarine melt rate. Nevertheless, future adaptations of

Figure S3. Network of flowlines on Kangerlussuaq Glacier, MEaSUREs Glacier ID 153, as defined with our tracing and filtering algorithm.

our method to simulate calving in larger-scale models may seek to add a mechanism for forcing by time-varying submarine melt. We suggest that those efforts begin by allowing submarine melt rate u_s to modify the terminus velocity, U in Equation 1, with the understanding that doing so may introduce scenarios that are incompatible with our original assumptions.

Text S5. Flowline network selection

We apply our depth-integrated, width-averaged model on a network of interacting glacier flowlines, as described in Ultee and Bassis (2017). Previous applications have used flowlines selected by hand (Ultee & Bassis, 2016; Ultee, 2018) or by an automated method that detects valley walls of mountain glacier networks (Kienholz et al., 2014; Ultee & Bassis, 2017). Neither method is suitable for the hundreds of Greenland outlet glaciers we consider here. It is impractical to select hundreds of flowlines by hand, and outlets of the Greenland Ice Sheet, unlike mountain glaciers, expand to a nearly featureless catchment upstream with no valley walls to aid in flowline selection. We therefore apply a new selection algorithm based on tracing ice surface velocity.

We begin with a surface velocity composite covering the entire ice sheet (ENVEO, 2017). For each glacier included in the MEaSUREs dataset (Joughin et al., 2015, updated 2017), we extract all points observed along the 2006 terminus position. We then trace each point up the surface velocity field until a pre-determined minimum velocity cutoff (identical for all glaciers); our viscoplastic approximation is most suitable near the glacier terminus (Ultee & Bassis, 2017; Bassis & Ultee, 2019), so we do not extend our simulated catchments all the way to the ice divide. Finally, we filter the set of full-length flowlines so that the most central flowline is defined as the "main trunk". The parallel portions of the remaining flowlines are trimmed and network intersections defined where the angle between flowlines exceeds a threshold value (identical for all glaciers). The code used in network selection is available in our public GitHub repository, and an example network is shown in Figure S3.

The tracing and filtering of flowlines from surface velocity is prone to error where the velocity dataset is noisy or includes holes. Errors in flowline tracing generally become apparent in later data-processing steps, for example if no optimal yield strength

value can be found. Networks affected by such errors include the note "Flagged for bad flowline trace" in Table S1.

Text S6. Detailed case studies

As described in the main article text, 40% of terminus positions simulated by SERMeQ fall within the range of observed terminus position for the same year. Because SERMeQ is sensitive to bed topography features (Ultee, 2018) and is forced by climate reanalysis data, model performance will generally be best where those data products are most accurate. The agreement between modelled and observed retreat of Sermeq Kujalleq (glacier ID 3, also called Jakobshavn Isbræ, main text Figure 3c), where bed topography has been especially well examined by previous glaciological studies, illustrates this point.

It is our aim to produce an upper bound on outlet glacier retreat and associated mass loss. We demonstrated in Bassis and Ultee (2019) that Equation 1 is a theoretical bound on the rate of calving retreat. Thus, we anticipate that the rate of retreat simulated by SERMeQ will generally exceed the observed rate of retreat. To support future implementation of this calving-rate bound in our model or others, it is important to understand where it does not perform as expected. There are two cases to consider: (1) the retreat rate simulated by SERMeQ is slower than the rate observed, or (2) the retreat rate simulated by SERMeQ far exceeds the rate observed (by a factor of 5 or more). We describe three illustrative examples here.

Mean simulated retreat slower than observed

Main text Figure 3a shows the simulated and observed changes in length for Apuseeq Anittangasikkaajuk (MEaSUREs Glacier ID 137), a small outlet glacier on the east coast of Greenland. Our analysis shows that the mean rate of simulated (single point) terminus retreat was 31 m/a, while the mean observed rate of retreat of the terminus centroid was 87 m/a. This is one of only a handful of cases in which the mean observed rate over the 2006-2014 period exceeds the supposed upper-bound rate produced by Equation 1. However, in this case both rates are small, and the simulated terminus position remains within the observed range of terminus positions. We also note that Apuseeq Anittangasikkaajuk is seldom included in other studies of Greenland outlets; as such, the quality of bed topography and climate data for this outlet may be relatively lower.

Mean simulated rate far exceeds observed

Main text Figure 3b shows the simulated and observed changes in length for Helheim Glacier (MEaSUREs Glacier ID 175), a large and well-studied outlet in southeast Greenland. The data quality for this outlet should be comparatively high. Nevertheless, SERMeQ simulates a mean retreat rate of 1980 m/a, which far exceeds the mean observed retreat rate of 313 m/a. We attribute this rapid retreat to features in the bed topography, combined with the no-flotation condition we have implemented in SERMeQ.

The terminus of Helheim Glacier has been observed to float in some years, and was likely floating at the beginning of our simulation period according to bed and surface topography from Morlighem et al. (2017). The glacier bed is more than 600 m below sea level and retrograde for several kilometers upstream of the present terminus, as shown in Figure S4. As explained in main text section 2 and in Ultee and Bassis (2016, 2017), SERMeQ does not allow floating ice tongues to form. Where small tongues are present, we remove them and simulate the first grounded point as the "terminus". In the case of Helheim Glacier, when we removed floating ice, the
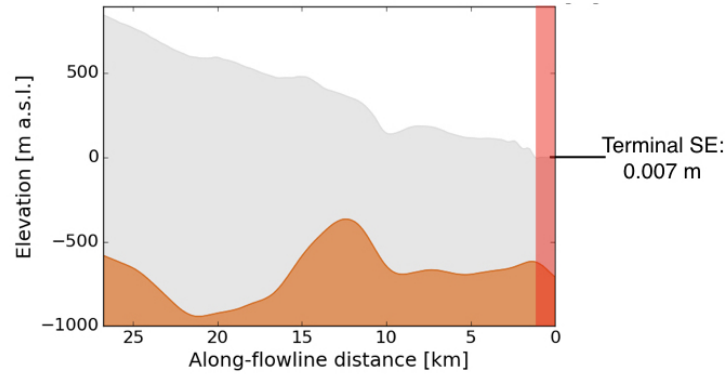
Figure S4. Near-terminus bed topography of Helheim Glacier. Brown filled region shows glacier bed and grey filled region shows glacier ice, both from Morlighem et al. (2017). Note 10:1 exaggeration in vertical scale. A red overlay indicates floating ice that was removed in our simulation. Annotation at figure left indicates the ice surface elevation at the terminus as recorded in Morlighem et al. (2017), further evidence that the initial terminus could not have been grounded ice.

simulated terminus was pushed onto the retrograde bed, where it began an unstable retreat. In summary, the true near-terminus dynamics and stress field of Helheim Glacier are shaped by the presence of floating ice that interacts with the fjord walls. SERMeQ does not include these dynamics and therefore simulates an upper-bound retreat that could occur in the absence of floating ice.

Successive under- and over-estimates within observed period

In a handful of other cases, the rate of retreat observed during a short period exceeds the rate simulated during the same period. Underestimated retreat in one time period is nearly always coupled with overestimated retreat in another period, such that the aggregate effect over the course of the simulation remains an upper-bound estimate of net retreat. For example, between 2007 and 2008, the floating ice tongue of Hagen Brae (MEaSUREs Glacier ID 105) disintegrated (Solgaard et al., 2020). The resulting observed rate of retreat, more than 10 km/a, far exceeded the rate simulated by SERMeQ (< 1 km/a) over the same period (Figure S4). However, our model initialization had already removed the floating portion of the glacier as of 2006, so the SERMeQ-simulated terminus position was still more retreated than the observed. In the subsequent period between 2008 and 2012, SERMeQ slightly overestimated the observed retreat rate. Figure S5 illustrates this history. In Figure S6, we have annotated the floating ice removed upon initialization, the collapse of which was responsible for anomalously high observed retreat between 2007 and 2008.

References

Balmforth, N. J., Craster, R. V., Rust, A. C., & Sassi, R. (2006). Viscoplastic flow over an inclined surface. *Journal of Non-Newtonian Fluid Mechanics*, *139*(1–2), 103 - 127. doi: 10.1016/j.jnnfm.2006.07.010

Bassis, J. N., & Ultee, L. (2019). A thin film viscoplastic theory for calving glaciers: Towards a bound on the calving rate of glaciers. *Journal of Geophysical Research: Earth Surface*, *124*. doi: 10.1029/2019JF005160
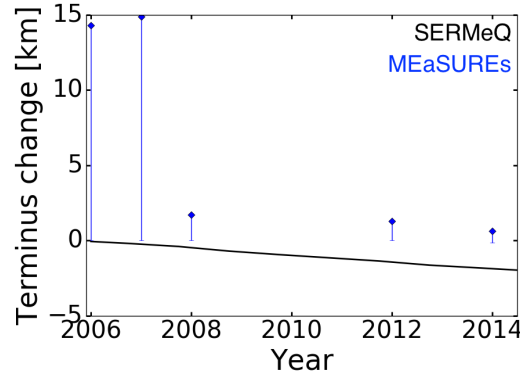
Figure S5. Observed and simulated change in terminus position on Hagen Brae (glacier ID 105). Black curves indicate SERMeQ-simulated terminus positions, while blue markers indicate MEaSUREs observations. The blue lines show the most-advanced and most-retreated parts of the terminus projected onto the centerline, and blue diamonds indicate the centroid of the observed terminus projected onto the centerline. Positive y-axis values indicate terminus positions more advanced than the initial position; negative y-axis values indicate terminus positions retreated from the initial position.
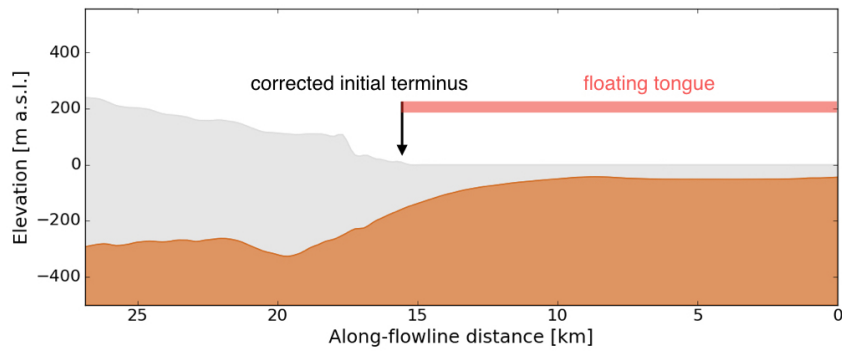

Figure S6. Near-terminus bed topography of Hagen Brae (glacier ID 105). Brown filled region shows glacier bed and grey filled region shows glacier ice, both from Morlighem et al. (2017). Note 10:1 exaggeration in vertical scale. A red bar shows the length of floating ice that was removed during our model initialization, and a black arrow indicates the first grounded point where SERMeQ could establish an initial terminus.

ENVEO. (2017). *Greenland ice velocity map 2016/2017 from Sentinel-1 [version 1.0]*. http://products.esa-icesheets-cci.org/products/details/greenland$_i ce_v elocity_m ap_w inter_2 016_2$

Joughin, I., Smith, B., Howat, I. M., & Scambos, T. (2015, updated 2017). *MEaSUREs Annual Greenland Outlet Glacier Terminus Positions from SAR Mosaics, Version 1.* NASA National Snow and Ice Data Center Distributed Active Archive Center. Boulder, Colorado USA. doi: https://doi.org/10.5067/DC0MLBOCL3EL

Kienholz, C., Rich, J. L., Arendt, A. A., & Hock, R. (2014). A new method for deriving glacier centerlines applied to glaciers in Alaska and northwest Canada. *The Cryosphere, 8*(2), 503–519. doi: 10.5194/tc-8-503-2014

Ma, Y. (2018). *Calving behavior of tidewater glaciers* (Doctoral dissertation, University of Michigan). Retrieved from https://deepblue.lib.umich.edu/handle/2027.42/146058

Ma, Y., & Bassis, J. N. (2019). The effect of submarine melting on calving from marine terminating glaciers. *Journal of Geophysical Research: Earth Surface, 124*(2), 334–346. doi: 10.1029/2018JF004820

Morlighem, M., Williams, C. N., Rignot, E., An, L., Arndt, J. E., Bamber, J. L., . . . Zinglersen, K. B. (2017). BedMachine v3: Complete bed topography and ocean bathymetry mapping of Greenland from multibeam echo sounding combined with mass conservation. *Geophysical Research Letters, 44*(21), 11,051-11,061. doi: 10.1002/2017GL074954

Nye, J. F. (1951). The flow of glaciers and ice-sheets as a problem in plasticity. *Proceedings of the Royal Society of London A: Mathematical, Physical and Engineering Sciences, 207*(1091), 554–572. doi: 10.1098/rspa.1951.0140

Solgaard, A. M., Simonsen, S. B., Grinsted, A., Mottram, R., Karlsson, N. B., Hansen, K., . . . Sørensen, L. S. (2020). Hagen Bræ: A surging glacier in North Greenland—35 years of observations. *Geophysical Research Letters, 47*(6), e2019GL085802. doi: 10.1029/2019GL085802

Ultee, L. (2018). *Constraints on the dynamic contribution to 21st-century sea level rise from Greenland outlet glaciers* (Doctoral dissertation, University of Michigan). Retrieved from https://deepblue.lib.umich.edu/handle/2027.42/145794

Ultee, L., & Bassis, J. N. (2016). The future is Nye: An extension of the perfect plastic approximation to tidewater glaciers. *Journal of Glaciology, 62*(236), 1143-1152. doi: 10.1017/jog.2016.108

Ultee, L., & Bassis, J. N. (2017). A plastic network approach to model calving glacier advance and retreat. *Frontiers in Earth Science, 5*(24). doi: 10.3389/feart.2017.00024